The genome of the zoonotic malaria parasite *Plasmodium simium* reveals adaptions to host-switching

Tobias Mourier[1], Denise Anete Madureira de Alvarenga[2], Abhinav Kaushik[1], Anielle de Pina-Costa[3,4,5§], Francisco J. Guzmán-Vega[6§], Olga Douvropoulou[1§], Qingtian Guan[1§], Sarah Forrester[7], Filipe Vieira Santos de Abreu[3,8], Cesare Bianco Júnior[3,9], Julio Cesar de Souza Junior[10], Zelinda Maria Braga Hirano[10], Alcides Pissinatti[11], Silvia Bahadian Moreira[11], Maria de Fátima Ferreira-da-Cruz[3,9], Ricardo Lourenço de Oliveira[3,8], Stefan T. Arold[6,12], Daniel C. Jeffares[7], Patrícia Brasil[3,4], Cristiana Ferreira Alves de Brito[2], Richard Culleton[13], Cláudio Tadeu Daniel-Ribeiro[3,9†] & Arnab Pain[1,14,15†]

1) Pathogen Genomics Laboratory, Biological and Environmental Sciences and Engineering (BESE) Division, King Abdullah University of Science and Technology (KAUST), Thuwal, Saudi Arabia

2) Grupo de Pesquisa em Biologia Molecular e Imunologia da Malária, Fundação Oswaldo Cruz (Fiocruz), Belo Horizonte/MG, 30190-009, Brazil

3) Centro de Pesquisa, Diagnóstico e Treinamento em Malária (CPD-Mal), Fiocruz, Rio de Janeiro/RJ, 21040-360, Brazil

4) Laboratório de Pesquisa Clínica em Doenças Febris Agudas, Instituto Nacional de Infectologia Evandro Chagas, Fiocruz, Rio de Janeiro/RJ, 21040-360, Brazil

5) Centro Universitário Serra dos Órgãos (UNIFESO), Teresópolis/RJ, 25964-004, Brazil

6) Computational Bioscience Research Center, Biological and Environmental Sciences and Engineering (BESE) Division, King Abdullah University of Science and Technology (KAUST), Thuwal, Saudi Arabia

7) Department of Biology and York Biomedical Research Institute, University of York, Wentworth Way, York, YO10 5DD, U.K.

8) Laboratório de Mosquitos Transmissores de Hematozoários. Instituto Oswaldo Cruz (IOC), Fiocruz, Rio de Janeiro/RJ, 21040-360, Brazil

9) Laboratório de Pesquisa em Malária, IOC, Fiocruz, Rio de Janeiro/RJ, 21040-360, Brazil

10) Universidade Regional de Blumenau (FURB), Centro de Pesquisas Biológicas de Indaial (CEPESBI)/ Projeto bugio, Blumenau and Indaial, SC, Brazil.

11) Centro de Primatologia do Rio de Janeiro (CPRJ/Inea), 25940-000, Guapimirim, RJ, Brazil

12) Centre de Biochimie Structurale, CNRS, INSERM, Université de Montpellier, 34090 Montpellier, France
13) Malaria Unit, Department of Pathology, Institute of Tropical Medicine (NEKKEN), Nagasaki University, 1-12-4 Sakamoto, Nagasaki, 852-8523, Japan
14) Global Station for Zoonosis Control, Global Institution for Collaborative Research and Education (GI-CoRE), Hokkaido University, N20 W10 Kita-ku, Sapporo, Japan
15) Nuffield Division of Clinical Laboratory Sciences (NDCLS), University of Oxford, Headington, Oxford, OX3 9DU, UK

§) Contributed equally, arranged alphabetically
†) Corresponding authors

Summary

Plasmodium simium, a malaria parasite of non-human primates in the Atlantic forest region of Brazil was recently shown to cause zoonotic infection in humans in the region. Phylogenetic analyses based on the whole genome sequences of six *P. simium* isolates infecting humans and two isolates from brown howler monkeys revealed that *P. simium* is monophyletic within the broader diversity of South American *Plasmodium vivax*, consistent with the hypothesis that *P. simium* first infected non-human primates as a result of a host-switch from humans carrying *P. vivax*. We provide molecular evidence that the current zoonotic infections of people have likely resulted from multiple independent host switches, each seeded from a different monkey infection. Very low levels of genetic diversity within *P. simium* genomes and the absence of *P. simium*-*P. vivax* hybrids suggest that the *P. simium* population emerged recently and has subsequently experienced a period of independent evolution in Platyrrhini monkeys. We further find that Plasmodium Interspersed Repeat (PIR) genes, Plasmodium Helical Interspersed Subtelomeric (PHIST) genes and Tryptophan-Rich Antigens (TRAg) genes in *P. siumium* are genetically divergent from *P. vivax* and are enriched for non-synonymous single nucleotide polymorphisms, consistent with the rapid evolution of these genes. Analysis of genes involved in erythrocyte invasion revealed several notable differences between *P. vivax* and *P. simium*, including large deletions within the coding region of the Duffy Binding Protein 1 (DBP1) and Reticulocyte Binding Protein 2a (RBP2a) genes in *P. simium*. Genotyping of *P. simium* isolates from non-human primates (NHPs) and zoonotic

human infections showed that a precise deletion of 38 amino acids in DBP1 is exclusively present in all human infecting isolates, whereas non-human primate infecting isolates were polymorphic for the deletion. We speculate that these deletions in the parasite-encoded key erythrocyte invasion ligands and the additional rapid genetic changes have facilitated zoonotic transfer to humans. Non-human primate malaria parasites can be considered a reservoir of potential infectious human parasites that must be considered in any attempt of malaria elimination. The genome of *P. simium* will thus form an important basis for future functional characterizations on the mechanisms underlying malaria zoonosis.

Introduction

There are currently eight species of malaria parasites known to cause disease in humans; *Plasmodium falciparum*, *Plasmodium vivax*, *Plasmodium malariae*, *Plasmodium ovale curtisi*, *Plasmodium ovale wallikeri*, *Plasmodium knowlesi*, *Plasmodium cynomolgi* and *Plasmodium simium*. The latter three species are more commonly parasitic on non-human primates and have only relatively recently been shown to infect humans [1-3].

As interventions against human malaria parasites, particularly *P. falciparum* and *P. vivax,* continue to reduce their prevalence, the increasing importance of zoonotic malaria is becoming apparent. In countries currently moving towards the elimination of malaria, the presence of populations of potentially zoonotic parasites in non-human primates constitutes a significant obstacle.

The propensity of malaria parasites to switch hosts and the consequences of this for human health are underlined by the fact that both *P. vivax* and *P. falciparum* first arose as human pathogens as the result of host switches from great apes in Africa [4-6]. As contact between humans and the mosquitoes that feed on non-human primates increases due to habitat destruction and human encroachment into non-human primate habitats [7], there is increasing danger of zoonotic malaria transmission leading to the emergence of novel human malaria pathogens. Understanding how malaria parasites adapt to new hosts and new transmission environments allows assessment of the risks posed by novel zoonotic malaria outbreaks.

The clinical epidemiology of zoonotic malaria varies according to the parasite species involved and the demographics of the human-host population infected. Severe and lethal outcomes have been reported in people infected with *P. knowlesi* in Malaysia [8], whilst infection with *P. cynomolgi* in the same region appears to cause moderate/mild clinical symptoms [9]. Interestingly, both *P. knowlesi* and *P. cynomolgi* infections in the Mekong region appear less virulent than in Malaysia, and are often asymptomatic [3,10], and this may be due to the relative virulence of the parasite strains circulating there and/or differences in the susceptibility of the local human populations. As the parasites of non-human primates have co-evolved with and adapted to their monkey hosts, it is impossible to predict their potential pathogenesis in zoonotic human infections. The virulence of *P. falciparum*, for example, has been attributed to its relatively recent emergence as a human pathogen [11], which appears to have occurred following a single host transfer from a gorilla in Africa [5].

Eighty nine percent of the malaria infections in Brazil are caused by *P. vivax,* with over 99% of these cases occurring in the Amazonian region. This region accounts for almost 60% of the area of Brazil, and is home to 13% of the population (https://www.ibge.gov.br/). Of the 0.4% of cases registered outside the Amazon, around 90% occur in the Atlantic Forest, a region of tropical forest that extends along the Atlantic coast of Brazil, and are caused by an apparently mild, vivax-like malaria parasite transmitted by *Anopheles (Kerteszia) cruzii*, a mosquito species that breeds in the leaf axils of bromeliad plants [12].

Following a malaria outbreak in the Atlantic Forest of Rio de Janeiro in 2015/2016, it was shown that these infections were caused by the non-human primate malaria parasite *P. simium* [1]. DNA samples collected both from humans and non-human primates (NHPs) in the same region shared identical mitochondrial genome sequences, distinct from *P. vivax* isolates from anywhere in the world and identical to that of a *P. simium* parasite isolated from a monkey in the same region in 1966, and to all isolates of *P. simium* recovered from NHPs since [13,14].

It was previously thought that *Plasmodium vivax* became a parasite of humans following a host switch from macaques in Southeast Asia, due to its close phylogenetic relationship with a clade of parasites infecting monkeys in this region and due to the high genetic diversity among *P. vivax* isolates from Southeast Asia [15]. We now know, however, that it became a human parasite following a host switch from great apes in Africa [6]. It is likely that it was introduced to the Americas by European colonisers following Columbus' journey to the New

World in 1492. Indeed, present-day *P. vivax* in South America is closely related to a strain of the parasite present, historically, in Spain [16]. The genetic diversity of extant *P. vivax* in the Americas suggests multiple post-Columbian colonising events associated with the passage of infected people from various regions throughout the world [17]. There is some evidence to suggest that *P. vivax* parasites may also have been introduced to South America in pre-Columbian times, and may have contributed to the extensive genetic diversity of the parasite on this continent [17].

Plasmodium simium, a parasite of various species of Platyrrhini monkeys whose range is restricted to the Atlantic Forest of south and southeast Brazil [18], is genetically and morphologically similar to *P. vivax* [1,19-22]. Based on this similarity, it appears likely that *P. simium* originated as a parasite of monkeys in Brazil following a host switch from humans carrying *P. vivax*. The recent 2015/2016 outbreak of *P. simium* in the local human population of Rio de Janeiro's Atlantic Forest raises questions about the degree of divergence that has occurred between *P. vivax* and *P. simium*, and whether adaptation to monkeys has led to the evolution of a parasite with clinical relevance to human health that differs from that of *P. vivax*.

It is unclear whether the current outbreak of *P. simium* in the human population of Rio de Janeiro was the result of a single transfer of the parasite from a monkey to a human and its subsequent transfers between people, or whether multiple independent host switches have occurred, each seeded from a different monkey infection. Furthermore, the degree and nature of adaptation to a non-human primate host and a sylvatic transmission cycle that has occurred in *P. simium* following its anthroponotic origin is of relevance to the understanding of how malaria parasites adapt to new hosts. It is also of interest to determine whether the current, human-infecting *P. simium* parasites have recently undergone changes at the genomic level that have allowed them to infect people in this region, as it has previously been suggested that *P. simium* has historically lacked the ability to infect man [23].

In order to resolve these questions, and so to better understand the epidemiology and natural history of this emerging zoonotic parasite, we analysed the whole genome sequences of *P. simium* parasites isolated from both humans and non-human primates in the Atlantic Forest region of Rio de Janeiro.

Results

Genome assembly and phylogeny

From a single *P. simium* sample collected from Rio de Janeiro state in 2016 [1] short read sequences were obtained and assembled into a draft genome (see Supplementary Materials). The assembled genome consists of 2,192 scaffolds over 1kb with a combined size of 29 Mb (Table S1). Two scaffolds corresponding to the apicoplast and mitochondrial organelles are also identified (Figure S1). Gene content analysis showed an annotation completeness comparable to previously published *Plasmodium* assemblies (Figure S35). A phylogenetic tree constructed from 3,181 of 1:1 orthologs of the annotated *P. simium* protein-coding genes with *Plasmodium vivax, P. cynomolgi, P. coatneyi, P. knowlesi, P. malariae, P. falciparum, P. reichenowi,* and *P. gallinaceum* confirmed that *P. simium* is very closely related to *P. vivax* (Figure S2).

P. simium-P. vivax diversity analysis

To detect single nucleotide polymorphisms (SNPs) within the *P. vivax*/*P. simium* clade, short Illumina paired-end sequence reads were mapped onto the *P. vivax* P01 reference genome [24]. Reads were collected from eleven human *P. simium* samples, two monkey *P. simium* samples, two *P. vivax* samples from Brazilian Amazon, and a range of *P. vivax* strains representing a global distribution retrieved from the literature [25]. Including only SNPs with a minimum depth of five reads, a total of 232,780 SNPs were initially called across 79 samples. Sixteen samples were subsequently removed from further analysis primarily due to low coverage resulting in a total of 63 samples (Table S2, Table S3). Few SNP loci are covered across all samples, and to enable diversity analysis, we restrict all further analysis to the 124,968 SNPs for which data is available from at least 55 samples (Figure S3).

P. simium-P. vivax population analysis

A Principal Component Analysis (PCA) plot constructed from these genome-wide SNP loci showed a clear separation between American and Asian *P. vivax* samples as well as a distinct grouping of *P. simium* samples (Figure S4). The latter observation suggesting that both human and monkey *P. simium* samples form a single population that is genetically differentiated from other American *P. vivax* populations. A similar pattern is observed when performing a multidimensional scaling analysis of the SNP data (Figure S5). To enable a

202 phylogenetic approach, we constructed an alignment from the 124,968 SNP sites. In the
203 resulting phylogenetic tree, *P. vivax* strains generally clustered according to their geographical
204 origin, and the Asian and American samples were clearly separated (Figure 1A, a tree with
205 sample IDs is available in Figure S6). *P. simium* samples clustered as a monophyletic group
206 with Mexican vivax samples (Figure 1A), consistent with a recent American origin for *P.*
207 *simium.*
208
209 To examine whether the *P. simium* isolates we obtained were part of a continuous population
210 with local *P. vivax*, we examined population ancestry with the ADMIXTURE program [26]
211 (Figure S7). This analysis is consistent with the PCA and MDS analysis (Figure S4 & Figure
212 S5) and the phylogenetic analysis of segregating SNPs (Figure 1), showing that *P. simium*
213 forms a genetically distinct population of *P. vivax*. The absence of *P. simium-P. vivax* hybrids
214 (introgression events) suggests that *P. simium* has undergone a period of independent
215 evolution in Platyrrhini monkeys.
216
217 ***P. simium* genetic differentiation from *P. vivax* is enhanced in host-parasite interacting**
218 **genes**
219 To characterise the *P. simium* population further, we estimated the nucleotide diversity in *P.*
220 *simium* and *P. vivax* samples (see Materials and Methods). *P. simium* diversity (genome-
221 median: 1.3×10^{-4}) is more than five times lower than the diversity observed when comparing
222 all *P. vivax* samples (genome-median: 7.5×10^{-4}) (Figure 2). Diversity within coding sequences
223 in *P. vivax* is consistent with previous reports [6]. The median nucleotide diversity between *P.*
224 *simium* and *P. vivax* genomes of 8.4×10^{-4} and the low diversity within *P. simium* suggest that
225 the strains we examined are part of a relatively recent or isolated population.
226
227 We then examined the population differentiation over the entire genome using $F_{ST,}$ a measure
228 of the proportion of ancestry private to a population (F_{ST}=0 for completely intermixed
229 populations, F_{ST}=1 for populations with completely independent ancestry). Although our
230 analysis contains very few samples, F_{ST} estimates can be very accurate if multiple genomic
231 sites are used [27]. Consistent with phylogenetic and admixture analysis, we observed a high
232 level of differentiation between human *P. simium* and American *P. vivax* (F_{ST}=0.46). For
233 comparison, the differentiation between vivax from America and vivax from Myanmar and
234 Thailand (henceforth referred to as 'Asian vivax') is less than half of this (F_{ST}=0.22). To
235 examine whether there were any signals of adaptive change in *P. simium* that may have

236 occurred during its adaptation in monkeys upon anthroponotic transfer, we calculated the
237 fixation index for all individual genes. Clearly, the small number of samples renders this
238 analysis prone to false and incorrect signals, and F_{ST} values for individual genes should be
239 interpreted with caution. Nevertheless, we attempted to look for general patterns in F_{ST} values
240 across gene groups.
241
242 Amongst the 4,341 *P. vivax* genes with at least one SNP in our data set, we examined the top-
243 25% of the genes with highest F_{ST} values for enrichment in functional Gene Ontology (GO)
244 terms or metabolic pathways. No GO terms or pathways were significant at the 0.05 level
245 after Bonferroni correction (Table S4 & Table S5). Using the *P. falciparum* orthologs instead
246 – when available – gave similar results (not shown). We next tested if any of the gene families
247 (Figure S8, Figure S9, Table S6) were associated with high F_{ST} values. Genes belonging to
248 the Plasmodium Interspersed Repeat (PIR) family involved in antigenic variation [28], the
249 Plasmodium Helical Interspersed Subtelomeric (PHIST) genes, a family of exported proteins
250 [29], the merozoite surface proteins MSP7[30], and Tryptophan-rich antigens (TRAg) [31] were
251 enriched among the genes with high F_{ST} values (binomial distribution, PIR; $p=3.5\times10^{-3}$,
252 PHIST; $p=4.1\times10^{-4}$, MSP7; $p=0.034$, TRAg; $p=2.5\times10^{-3}$).
253
254 As these gene families are involved in parasite-host interactions, the observation of elevated
255 F_{ST} values may simply reflect a general pattern of rapid genetic divergence in *Plasmodium*
256 parasites. To test this, we repeated the F_{ST} analysis between American vivax and a selection of
257 Asian vivax isolates (Myanmar and Thailand samples only). Consistent with the phylogenetic
258 analysis (Figure 1A) gene F_{ST} was slightly higher overall between simium and American
259 vivax than between American and Asian vivax samples (Figure 3A). However, none of the
260 gene families were overrepresented among genes with high F_{ST} (top-25%) between American
261 and Asian vivax. To further examine if the elevated F_{ST} measures found for PIR, PHIST,
262 MSP7, and TRAg genes are exclusive to the comparison between simium and American
263 vivax, we calculated the ratio between the two F_{ST} measurements ('simium versus American
264 vivax' and ' American versus Asian vivax') (Figure 3B). The ratios for PIR, PHIST and TRAg
265 genes were significantly higher than observed for the remaining genes (Figure 3C), whereas
266 ratios for MSP7 genes were not (Mann-Whitney U, p=0.12). Although the *P. simium* and the
267 *P. vivax* P01 both genomes encode a high number of the gene family members, our analysis is
268 restricted to the *P. vivax* genes for which our *P. simium* short read sequences can map. For
269 example, only 408 out of the 1209 *P. vivax* PIR genes have coverage from *P. simium* reads

270 across at least 80% of their gene length (Figure S10). Further, an even smaller number of
271 these genes have detectable SNPs between simium and American vivax samples and are
272 included in the analysis (numbers shown below Figure 3B).
273
274 To test if the sequence redundancy among gene family loci could result in spurious cross-
275 mapping of short sequence reads we specifically tested the quality of SNPs in gene families,
276 and SNPs residing in gene families showed no signs of decreased calling, mapping, or base
277 qualities compared to other SNPs (Figure S11).
278
279 A phylogenetic analysis of PIR, PHIST and TRAg proteins harbouring genomic SNPs
280 revealed no apparent association between certain protein phylogenetic sub-groups and high
281 F_{ST} ratios (Figure S12-S14), consistent with a subtle signature of polygenic adaptation in
282 these gene families.
283
284 When testing all exported genes and genes involved in invasion and exported genes (Table
285 S8), the observed F_{ST} ratios were not significantly different from the background (Mann-
286 Whitney U, p=0.5473). Hence, the differences in F_{ST} observed for PIR, PHIST and TRAg
287 genes are not a general phenomenon amongst the genes known to be involved in interactions
288 with the host and red cell invasion.
289
290 The observed skew towards higher F_{ST} values when comparing simium and American vivax
291 (Figure 3A) could be a result of an inherent diversity between different American vivax
292 populations potentially stemming from multiple introductions of *P. vivax* to the American
293 continent [17]. To test if such founder effects and subsequent population bottlenecks could
294 explain the observations, we repeated the F_{ST} analysis using only Mexican vivax samples as
295 American representatives. Four Mexican samples (SRS693273, SRS694229, SRS694244,
296 SRS694267) were used. These clustered close together in both the SNP phylogeny (Figure 1)
297 and in the PCA and MDS plots (Figure S4 & Figure S5), and are assumed to share a recent
298 evolutionary history. This analysis revealed the same pattern of elevated F_{ST} values between
299 simium and Mexican vivax, and PIR genes did again display significantly higher F_{ST} ratios
300 (Figure S15). Although PHIST and TRAg genes also showed higher F_{ST} ratios, these were no
301 longer significant (Figure S15). We therefore conclude that the observed higher F_{ST} values
302 between simium and American vivax PIR genes are not solely a result of diversity within
303 American vivax populations, but rather appear specific to comparisons with *P. simium*.

304

305 Adaptive changes in PIR genes would be expected to produce stronger genetic divergence in
306 non-synonymous codon positions. To examine this, we divided genic SNPs into synonymous
307 and non-synonymous changes. In PIR genes, there are 353 non-synonymous and 185
308 synonymous SNPs (non-synonymous to synonymous SNP ratio = 1:1.91). Similarly, in
309 PHIST and TRAg genes we find 220 and 103 non-synonymous, respectively, and 67 and 41
310 synonymous SNPs, respectively (PHIST ratio = 1:3.28, TRAg ratio = 1:2.51). In all other
311 genes, the ratio between non-synonymous and synonymous SNPs is 1:1.49. Hence, the
312 proportion of non-synonymous SNPs in PIR, PHIST and TRAg genes is significantly higher
313 than in all other genes (chi-square, PIR; p= 0.0073, PHIST; $p=9.4\times10^{-9}$, TRAg; p=0.0054).

314

315 Our finding that PIR, PHIST and TRAg genes overall display markedly higher F_{ST} values
316 between simium and vivax suggest that these gene groups are enriched for private alleles
317 consistent with natural selection acting upon these genes subsequent to the split between *P.*
318 *simium* and *P. vivax*.

319

320 ***P. simium* invasome components**

321 In invading *P. vivax* merozoites, binding to host red blood cells is mediated by two gene
322 families: Duffy Binding Proteins (DBPs) bind the Duffy Antigen Receptor for Chemokines
323 (DARC) [32,33], which is present on both host normocytes and reticulocytes, whereas
324 Reticulocyte Binding Proteins (RBPs) preferentially bind host reticulocytes [34-36]. Recently, the
325 reported protein structure of *P. vivax* RBP2b revealed the evolutionary conservation of
326 residues involved in the invasion complex formation [36]. Two DBPs, DBP1 and DBP2, are
327 present in *P. vivax* P01 (Table S9). RBPs can be divided into three subfamilies, RBP1, RBP2,
328 and RBP3 [37]. The *P. vivax* P01 genome encodes 11 RBPs (including the reticulocyte binding
329 surface protein, RBSA), of which three are pseudogenes (Table S9).

330

331 The *P. vivax* DBP and RBP were used to search the *P. simium* proteins, resulting in the
332 detection of the two DBP proteins and RBP1a, RBP1b, RBP2a, RBP2b, and RBP3 and failure
333 to detect RBP2c and RBP2d (Figure 4; Table S9; Figure S16; Figure S17) across all
334 sequenced *P. simium* samples. As in other *P. vivax* genomes, the *P. simium* RBP3 is a
335 pseudogene [38], indicating that the pseudogenization event happened prior to the split between
336 *P. vivax* and *P. simium*.

337

338 To determine whether the apparent absences of individual RBP genes in *P. simium* were due
339 to incomplete genome assembly, we examined the coverage of *P. simium* reads mapped onto
340 *P. vivax* RBP gene loci. As expected, no *P. simium* coverage was observed at the RBP2c,
341 RBP2d, and RBP2e genes in *P. simium* samples, including the previously published CDC
342 strain deposited in GenBank (accession ACB42432) [39] (Figure S18).
343
344 Coverage of mapped reads across invasome gene loci revealed no apparent elevated coverage
345 in genes compared to their flanking genomic regions, which would otherwise be expected if
346 the *P. simium* genome contained multiple (duplicated) copies of non-assembled invasion
347 genes (Figure S19). Similarly, analysis of *P. simium* read mapping data using the DELLY
348 software [40] showed no large genomic duplications and deletions events occurring at loci
349 harbouring invasion genes (Table S10) although numerous short indels were detected within
350 protein-coding genes (Table S11).
351
352 **Structural variation in *P. simium* Duffy Binding Protein 1**
353 The simium assembly revealed that the invasion gene DBP1 contains a large deletion within
354 its coding sequence (Figure 4) (a full alignment is provided in Figure S20). Intriguingly, the
355 previously published *P. simium* CDC strain (originally isolated in 1966) DBP1 does not
356 contain the deletion ('simium CDC' in Figure 4B). A haplotype network confirms that this
357 previously published DBP1 gene is indeed a *P. simium* sequence (Figure S22), and the SNP
358 analyses consistently assign the CDC strain to the simium cluster (Figure 1, Figure S4, and
359 Figure S5). Compared to the *P. vivax* P01 reference genome the SalI reference harbours a 27
360 base pair deletion in DBP1, in contrast to the 115 bp deletion observed in all *P. simium*
361 samples isolated from humans (Figure 4). This deletion is also present in most *P. vivax*
362 isolates (Figure S23). Additional deletion patterns exist among isolates, and in a few cases
363 multiple versions are detected within samples (Figure S23).
364
365 The presence of repetitive sequences within the DBP1 gene could potentially result in
366 aberrant assembly across the DBP1 locus, which could appear as an apparent deletion in
367 subsequent bioinformatic analysis. We tested this possibility and the DBP1 gene does not
368 harbour any noticeable degree of repetitiveness (Figure S24). Several read mapping analyses
369 confirmed that the *P. simium*-specific 115 bp deletion was not an assembly artefact (Figure
370 S25-S27).
371

372 We next designed primers for PCR amplification of a genomic segment across the deleted
373 region in the *P. simium* DBP1 gene and tested the occurrence of these deletion events in a
374 range of *P. vivax* and *P. simium* field samples from Brazil. All *P. vivax* samples tested by
375 PCR produced bands consistent with absence of the deletion whereas all samples from
376 human-infecting *P. simium* produced bands consistent with the presence of the precise 115 bp
377 deletion (Figure S28, top & middle). Interestingly, non-human primate (NHP)-infecting *P.*
378 *simium* isolates were a mix of samples with and without deletions (Figure S28, bottom). If the
379 *P. simium*-specific deletion in DBP1 is a prerequisite for the ability to infect humans this
380 suggests that only a subset of NHP-infecting *P. simium* parasites currently possess the DBP1
381 allele required for zoonotic transfer to humans.
382
383 A large, additional deletion was observed in the *P. simium* RBP2a gene, the presence of
384 which was also supported by read mapping and PCR analysis (Figure 3, Figure S29-S32).
385
386
Potential structural implications of the deletion in DBP1 and RBP2a
387 We next investigated if the observed deletions render DBP1 and RBP2a dysfunctional. DBP1
388 contains a large extracellular region, which includes the N-terminal DBL region which is
389 mediating the association with DARC in *P. vivax* [41], followed by a largely disordered region
390 and a cysteine-rich domain (Figure 4c). DBP1 has a single-pass transmembrane helix and a
391 short cytoplasmic tail. The deletion observed in the human-infecting *P. simium* only affects
392 the disordered region, leaving the flanking domains intact. We produced homology models of
393 the DBL domains from the *P. vivax* strain P01, the human-infecting *P. simium* strain AF22,
394 and the *P. simium* CDC strain, based on the crystal structure of the >96% identical DBL
395 domain of *P. vivax* bound to DARC (PDB ID 4nuv). Whereas no significant substitutions
396 were found in the DBL domain between both *P. simium* sequences, our analysis showed that
397 residue substitutions between *P. simium* and *P. vivax* DBL domains cluster in proximity of the
398 DARC binding site (Figure S33). Based on our models, these substitutions are unlikely to
399 negatively affect the association with DARC, supporting that the DBL domains of both *P.*
400 *simium* would be capable of binding to human DARC. Hence, the human-infecting *P. simium*
401 sequence encodes for a protein that retains the capacity to bind to human DARC, but would
402 have the interacting domain positioned closer to the membrane than in the monkey-infecting
403 CDC strain.
404

405 The deletion we detected in human-infecting RBP2a was more severe, resulting in the loss of
406 1003 residues. These residues are predicted to form a mostly α-helical extracellular stem-like
407 structure that positions the reticulocyte binding domain away from the membrane (Figure 4d).
408 However, given that the deletion does neither affect the transmembrane region, nor the
409 receptor-binding domain, our analysis supports that the resulting truncated RBP2a protein can
410 still associate with the human receptor, but that the binding event would occur closer to the
411 plasmodium membrane.
412
413
414

Discussion

415
416 We present the genome of *Plasmodium simium*, the eighth malaria parasite species known to
417 infect humans in nature. In recent evolutionary time, *P. simium* has undergone both
418 anthroponosis and zoonosis making it unique for the study of the genetics underlying host-
419 switching in malaria parasites. The genome content confirmed the close phylogenetic
420 relationship between *P. simium* and *P. vivax*, and further analyses on single nucleotide
421 divergences support a very recent American origin for *P. simium.* This recent split between *P.*
422 *vivax* and *P. simium* precludes detection of genes under positive evolution [42], and we have
423 instead performed a general analysis of population differentiation between extant *P. simium*
424 and *P. vivax* isolates using F_{ST}. We find that members of three gene families involved in
425 antigenic variation, PIR, PHIST and TRAg, show significantly elevated F_{ST} levels between *P.*
426 *simium* and *P. vivax*. As higher F_{ST} values amongst these genes are not observed between
427 global vivax populations, their genetic differentiation appears to be associated with host-
428 switching between human and monkey.
429
430
431 Two proteins involved in host invasion, DBP1 and RBP2a, were found to harbour extensive
432 deletions in *P. simium* compared to *P. vivax*. Interestingly, experimental analysis of *P. simium*
433 samples revealed that isolates from human hosts all carried the DBP1 deletion, whereas
434 isolates from non-human primates displayed both absence and presence of the deletion. This
435 DBP1 deletion is not present in the *P. simium* isolated from a brown howler monkey in the
436 1960s, which was previously shown to be incapable of infecting humans [23], although some
437 degree of laboratory adaptation of this parasite may have affected its genome. However, this
deletion is also absent in *P. vivax*, so cannot in itself explain the ability of *P. simium* to infect

438
439 humans in the current outbreak. It is possible, however, that this deletion is required for *P.*
440 *simium* to invade human red blood cells given the alterations that have occurred elsewhere in
441 its invasome following adaptation to non-human primates since the split between *P. simium*
442 and its human-infecting *P. vivax* ancestor.
443
444 Invasome proteins are obvious candidates for genetic factors underlying host-specificity, and
445 an inactivating mutation in a *P. falciparum* erythrocyte binding antigen has recently been
446 shown to underlie host-specificity [43]. Traditionally, functional studies on invasome proteins
447 have focused on domains known to bind or interact directly with the host. Although the *P.*
448 *simium*-specific DBP1 and RBP2a deletions reported here do not cover known structural
449 motifs, these deletions could nevertheless affect host cell recognition as disordered protein
450 regions have known roles in cellular regulation and signal transduction [44]. Further, a shorter,
451 less flexible linker between the plasmodium membrane and the receptor-binding DBP1
452 domain may favour a more rigid and better oriented positioning of the dimeric DBP1,
453 enhancing its capacity to engage the human receptor.
454
455 Phylogenetic analysis of the *P. simium* clade gives the geographical location of its most
456 closely related *P. vivax* strain as Mexico, and not Brazil. In imported populations, the
457 relationship between geographical and genetic proximity may be weak. Multiple introductions
458 of diverse strains from founder populations may occur independently over large distances, so
459 that two closely related strains may be introduced in distantly located regions. It may be
460 postulated that there occurred the introduction of strains of *P. vivax* to Mexico from the Old
461 World that were closely related, due to similar regions of origin, to strains introduced to the
462 Atlantic Forest which went on to become *P. simium* in New World monkeys. Strains from a
463 different point of origin were introduced to the Amazonian region of Brazil. This hypothesis
464 necessitates reproductive isolation of the *P. simium* clade from the Brazilian *P. vivax* parasites
465 following their initial introduction; an isolation that would be facilitated, presumably, by their
466 separate host ranges.
467
468 Due to uncertainties regarding the number of individual genomes that were transferred during
469 the original host switch from man to NHPs that resulted in the formation of the *P. simium*
470 clade, it is impossible to perform dating analyses to determine a time for the split between *P.*
471 *vivax* and *P. simium* with which we can be confident. The phylogeny shown in figure 1 is
consistent with the hypothesis that all present-day *P. vivax*/*P. simium* originated from a now

extinct Old World population. The most parsimonious explanation for this is that today's New World *P. vivax/P. simium* originated from European *P. vivax*, which was itself a remnant of the original Eurasian/African *P. vivax* driven to extinction in Africa by the evolution of the Duffy negative condition in the local human populations, and from Europe by malaria eradication programmes in the latter half of the twentieth century. This hypothesis is supported by the evidence of a close relationship between historical Spanish *P. vivax* and South American strains of the parasite [16], and by previous analyses of the mitochondrial genome [45]. Therefore, we postulate that the host switch between humans and non-human primates that eventually led to establishment of *P. simium* in howler monkeys must have occurred subsequent to the European colonisation of the Americas, within the last 600 years.

We find no evidence from the nuclear genome, the mitochondrial genome or the apicoplast genome that any of the *P. vivax /P. simium* strains from the New World considered in our analyses are more closely related to Old World parasites than they are to each other, as previously contended [46]. However, our nuclear genome phylogeny is based on genome-wide SNPs, and so represents an "average" phylogeny across the genome. This cannot be considered to reflect a true history of parasite ancestry due to the effects of recombination, and it is possible that trees produced from individual genes might reveal different phylogenetic relationships.

Given the limited genetic diversity amongst the *P. simium* isolates considered here compared to that of *P. vivax*, it is almost certain that the original host switch occurred from humans to NHPs, and not the other way around [22]. Similarly, the larger amount of genetic diversity in the current NHP-infecting *P. simium* compared to those *P. simium* strains isolated from humans (as indicated by the higher degree of DBP1 polymorphism in the NHP-infecting *P. simium* compared to the strains infecting humans), suggests that humans are being infected from a pool of NHP parasites in a true zoonotic manner, as opposed to the sharing of a common parasite pool between humans and NHPs

The biological definition of a species is a group of organisms that can exchange genetic material and produce viable offspring. We have no way of knowing whether this is the case for *P. vivax* and *P. simium*, and genetic crossing experiments would be required to resolve this question. Our phylogenetic analysis, however, clearly shows *P. simium* forming a clade on its own within the broader diversity of *P. vivax*, and that strongly suggests, given what we know

about its biology, that allopatric speciation has been/is occurring. *Plasmodium simium* appears to have been reproductively isolated from other strains of *P. vivax* for long enough for significant genetic differentiation to occur (F_{ST} = 0.46), with some invasome genes showing even higher genetic differentiation.

Plasmodium simium is currently recognised as a species separate from *P. vivax*; it has been well characterised and described in the literature, and there is a type specimen available, with which all the strains sequenced here cluster in one monophyletic group. Therefore, we cannot at present overturn the species status of *P. simium* in the absence of conclusive proof from crossing experiments.

In summary, the recent outbreak of human malaria in the Atlantic Forest of Rio de Janeiro underlines the impact of zoonotic events on human health. In this sense non-human primate malaria parasites can be considered a reservoir of potential infectious human parasites that must be considered in any attempt of malaria eradication. Little is known about the genetic basis for zoonosis, yet the presented genome sequence of *P. simium* suggests a deletion within the DBP1 gene as a possible facilitator of zoonotic transfer. The genome of *P. simium* will thus form an important basis for future functional characterizations on the mechanisms underlying malaria zoonosis.

Methods

Sample Collection and Preparation

Human and primate samples of *P. simium* were collected and prepared as part of a previous study [1,14]. Additionally, two *P. vivax* samples from the Amazon area of Brazil were also collected from human patients (Table S2). All participants provided informed written consent. The *P. simium* CDC (Howler) strain (Catalog No. MRA-353) from ATCC was obtained via the BEI Resources Repository in NIAID-NIH (https://www.beiresources.org/).

DNA extraction and sequencing

DNA was extracted as described[1]. The genomic DNA for each sample was quantitated using the Qubit® 2.0 Fluorometer and was used for library preparation. The DNA for intact samples was sheared using a Covaris E220 DNA sonicator to fragments of 500bp. The DNA libraries

540 for intact samples were made using the TruSeq Nano DNA Library Prep kit (Illumina),
541 whereas the DNA libraries for degraded samples were made using Ovation Ultralow Library
542 System V2 kit (Nugen), according to the manufacturers' instructions. The amplified libraries
543 were stored in -20 °C. The pooled libraries were sequenced in an Illumina HiSeq4000
544 instrument (2 x 150 bp PE reads) (Illumina). A PhiX control library was applied to the
545 sequencing run as a base balanced sequence for the calibration of the instrument so that each
546 base type is captured during the entire run. Raw sequence reads were submitted to FastQC
547 v.0.11.5 and the quality score of the sequences generated was determined. Samples AF22,
548 AF26, AF36 were additionally sequenced and scaffolded by PacBio RS II platform (Pacific
549 Biosciences, California, US) using a SMRT library. Genomic DNA from the *P. vivax* samples
550 was extracted from filter paper as previously described [47].
551
552 **Illumina reads preparation and mapping**
553 Fastqc v 0.11.6 (http://www.bioinformatics.babraham.ac.uk/projects/fastqc) was used to
554 evaluate the quality of Illumina reads. Illumina adapters were removed, and reads were
555 trimmed using the trimmomatic v0.33 [48] software with the following conditions:
556 *LEADING:20 TRAILING:20 SLIDINGWINDOW:4:20 MINLEN:36*
557 To exclude human reads from our analysis, trimmed reads were mapped against the human
558 reference genome (v. hg38) and the *Plasmodium vivax* strain P01 reference genome (v. 36)
559 from PlasmoDB (www.plasmodb.org) with bowtie2 (v 2.3.3.1) [49]. Reads mapping against the
560 human genome were removed from further analysis.
561
562 **Genome Assembly**
563
564 *P. simium* sample AF22 was selected for genome assembly based on read quality and
565 coverage. After removal of human contaminants, Illumina reads were assembled into contigs
566 using the Spades (v 3.70) assembler [50]. Contigs assembled into scaffolds running SSPACE (v
567 3.0) [51] for 15 rounds and gaps filled with Gapfiller (v 1.10) [52]. Scaffolds were subsequently
568 corrected with Illumina reads using the Pilon (v 1.22) software [53]. Blobtools (v 1.0) (DOI:
569 10.5281/zenodo.845347) [54] was used to remove any residual contaminant scaffolds. Genome
570 size and GC content is in line with that of *P. vivax* species (Table S1). Genomic scaffolds
571 representing the mitochondrial and apicoplast genome were identified through blastn searches
572 against the corresponding *P. falciparum* and *P. vivax* sequences (Figure S1). The *P. simium*
573 mitochondrial genome was aligned against a range of previously published *P. vivax* and *P.*
simium mitochondrial genomes [55,56]. A gap-filled region in the alignment where the distal

parts of the *P. simium* scaffold were merged was manually deleted. A minimum spanning haplotype network was produced using PopART [57,58] confirming the authenticity of the *P. simium* mitochondrial genome (Figure S34).

Genome Annotation

Two approaches were used to annotate the reference *P. simium* AF22 genome. Firstly, the Maker pipeline (v 2.31.8) [59] was run for two rounds, using ESTs and protein evidence from *P. vivax* and *P. cynomolgi* strain B and *P. falciparum* to generate Augustus gene models. Secondly, a separate annotation was produced using the Companion web server [60]. Companion was run using the *P. vivax* P01 reference assembly and default parameters. Basic annotation statistics are provided in Table S1. The relatively low number of genes (5966) is lower due to the fragmented and incomplete nature of the *P. simium* assembly (Table S1). Gene content was estimated using BUSCO [61,62] (v3.0) revealing an annotation completeness comparable to other Plasmodium genome assemblies (Figure S35).

PlasmoDB Genome References and Annotations

Genome fasta files, as well as annotated protein and CDS files were obtained from PlasmoDB for the following species: *P. gallinaceum* 8A, *P. cynomolgi* B and M, *P knowlesi* H, *P. falciparum* 3D7, *P. reichenowi* G01, *P. malariae* UG01, *P. ovale curtisi* GH01, *P. coatneyi* Hackeri, *P. vivax* P01 and *P. vivax* SalI. For each species, version 36 was used.

Orthologous group determination

Amino-acid sequences-based phylogenetic trees were prepared using protein sequences from the *P. simium* annotation, as well as the protein annotations from 10 malaria species downloaded from PlasmoDB: *P. vivax* P01, *P. cynomolgi* B, *P. knowlesi* H, *P. vivax*-like Pvl01, *P. coatneyi* Hackeri, *P. falciparum* 3D7, *P. gallinaceum* 8A, *P. malariae* UG01, *P. ovale* curtisi GH01, and *P. reichenowi* G01. *P. vivax*-like from PlasmoDB version 43, all other annotations from version 41. A total of 3181 1:1 orthologous genes were identified using the Proteinortho (v 6.0.3) software [63]. Approximately 88% of the predicted genes in *P. simium* have orthologs in the *P. vivax* P01 (Figure S36).

Indels in genes

Structural variations were detected using DELLY [40] (v 0.7.9). Coordinates of structural rearrangements their nearest genes are listed in Table S10. Shorter indels were detected from

608 soft-clipping information in read mapping (using the '-i' option in DELLY)(Table S11). Indels
609 in exons were further compared to indels present in the *P. simium* AF22 genome assembly,
610 suggesting a high false discovery rate of DELLY indels compared to assembly indels (Figure
611 S37).
612
613 **Protein phylogeny**
614 Protein sequences were aligned using mafft (v 7.222) [64] and alignments were subsequently
615 trimmed with trimAl (v 1.2rev59) [65] using the heuristic 'automated1' method to select the best
616 trimming procedure. Trimmed alignments were concatenated and a phylogenetic tree was
617 constructed using RAxML (v 8.2.3) [66] with the PROTGAMMALG model.
618
619 **SNP calling and analysis**
620 Short sequence reads from 15 simium samples (13 human and 2 monkey) and two vivax
621 samples, all from this study (Table S2), were aligned against a combined human (hg38) and
622 *P. vivax* (strain P01, version 39) genome using NextGenMap (v0.5.5) [67]. This was similarly
623 done for 30 previously published *P. vivax* strains [25] and the Sal1 reference. These data sets
624 were downloaded from ENA (https://www.ebi.ac.uk/ena) (Table S3).
625 Duplicate reads were removed using samtools (v 1.9) [68] and the filtered reads were realigned
626 using IndelRealigner from the GATK package (v 4.0.11) [69]. SNPs were called independently
627 with GATK HaplotypeCaller and freebayes (v 1.2.0) [70], keeping only SNPs with a QUAL
628 score above 30. The final SNP set were determined from the inter-section between GATK and
629 freebayes. Allele frequencies and mean coverage across SNP sites are shown in Figure S38.
630 PCA plot was constructed using plink (v 1.90) [71], and admixture analysis was done with
631 Admixture (v 1.3.0) [26]. F_{ST} values were estimated from nucleotide data with the PopGenome
632 R package [72,73] using the Weir & Cockerham method [74]. Non-synonymous and synonymous
633 SNPs were identified using snpeff [75].
634
635 **SNP phylogeny**
636 Alleles from SNP positions with data in 55 samples were retrieved, concatenated, and aligned
637 using mafft [64]. Tree was produced by PhyML [76,77] with the GTR substitution model selected
638 by SMS [78]. Branch support was evaluated with the Bayesian-like transformation of
639 approximate likelihood ratio test, aBayes [79]. Phylogenetic network was made in SplitsTree [80]
640 using the NeighborNet network [81].
641

642 **Nucleotide diversity**

643 Conventional tools calculating nucleotide diversity directly from the variant call files assumes
644 that samples are aligned across the entire reference sequence. But as read coverage across the
645 reference genome was highly uneven between samples (Figure S38), adjustment for this was
646 required. Coverage across the reference genome was thus calculated for each sample using
647 samtools mpileup (v 1.9) [68]. For each comparison between two samples, the nucleotide
648 divergence was calculated as number of detected bi-allelic SNPs per nucleotide with read
649 coverage of at least 5X in both samples.

650

651 **Gene sequence deletions**

652 Exploratory Neighbor-Joining phylogenies produced with CLUSTALW [82,83] and visualized
653 with FigTree (https://github.com/rambaut/figtree/) after alignment with mafft [82]. Pacbio reads
654 were aligned using Blasr (v 5.3.2) [84], short Illumina reads using NextGenMap (v0.5.5) [67].
655 Dotplots done with FlexiDot (v1.05) [85].

656

657 **Gene families and groups**

658 Exported gene sets were compiled from the literature [86-88]. Invasion genes were retrieved from
659 [89]. Gene families were assessed in seven Plasmodium genomes (*P. simium*, *P. vivax* SalI, *P.*
660 *vivax* P01, *P. vivax-like* Pvl01, *P. cynomolgi* M, *P. cynomolgi* B, and *P. knowlesi* H) using the
661 following pipeline: For all genomes annotated genes were collected for each gene families.
662 These 'seed' sequences were used to search all proteins from all genomes using BLASTP and
663 best hits for all proteins were recorded. For each gene family 'seed' sequences were then
664 aligned with mafft [64], trimmed with trimAl [65], and HMM models were then built using
665 HMMer (http://hmmer.org/). For PIR/VIR and PHIST genes, models were built for each
666 genome independently, for all other gene families a single model was built from all genomes.
667 These models were then used to search all proteins in all genomes. All proteins with best
668 BLASTP hit to a 'seed' sequence from a given genome were sorted according to their bit
669 score. The lowest 5% of hits were discarded and remaining proteins with best hits to a 'seed'
670 sequence were assigned one 'significant' hit. As all proteins were searched against 'seeds' from
671 the six annotated genomes (P. simium excluded), a maximum of six 'significant' BLAST hits
672 could be obtained. Similarly, for each HMM model the bottom 25% hits were discarded and
673 remaining hits were considered 'significant'. The final set of gene families consists of
674 previously annotated genes and un-annotated genes with at least two 'significant' hits (either
675 BLASTP or HMM).

676

677

PCR amplification of DBP1 and RBP2a genes

678 PCR primers were initially designed from alignments between *P. vivax* and *P. simium*
679 sequences and subsequent tested using Primer-BLAST [90] and PlasmoDB
680 (www.plasmodb.org). For DBP1, the reaction was performed in 10 μL volumes containing
681 0.5 μM of each oligonucleotide primer, 1 μL DNA and 5 μL of Master Mix 2x (Promega)
682 (0.3 units of Taq Polymerase, 200 μM each deoxyribonucleotide triphosphates and 1.5 mM
683 MgCl2). Samples were run with the following settings: 2 minutes of activation at 95°C,
684 followed by 35 cycles with 30 seconds denaturation at 95°C, 30 seconds annealing at 57°C
685 (ΔT=-0.2 °C from 2nd cycle) and 1 minute extension at 72°C, then 5 minutes final extension
686 at 72°C and hold in 4°C. For RBP2a PCR, the reaction was performed in 10 μL volumes
687 containing 0.5 μM of each oligonucleotide primer, 1 μL DNA, 0.1 μL PlatinumTaq DNA
688 Polymerase High Fidelity (Invitrogen, 5U/ μL), 0.2 mM each deoxyribonucleotide
689 triphosphates and 2 mM $MgSO_4$. The PCR assays were performed with the following cycling
690 parameters: an initial denaturation at 94°C for 1.5 min followed by 40 cycles of denaturation
691 at 94°C for 15 sec, annealing at 65°C for 30 sec (ΔT=-0.2 °C from 2nd cycle) and extension at
692 68°C for 3.5 min. The temperature was then reduced to 4 °C until the samples were taken. All
693 Genotyping assays were performed in the thermocycler Veriti 96 wells, Applied Biosystems,
694 and the amplified fragments were visualized by electrophoresis on agarose gels (2% for DBP1
695 and 1% for RBP2a) in 1x TAE buffer (40 mM Tris-acetate, 1 mM EDTA) with 5 μg/ mL
696 ethidium bromide (Invitrogen) in a horizontal system (Bio-Rad) at 100 V for 30 min. Gels
697 were examined with a UV transilluminator (UVP - Bio-Doc System).

698

699

700 To prevent cross-contamination, the DNA extraction and mix preparation were performed in
701 "parasite DNA-free rooms" distinct from each other. Furthermore, each of these separate
702 areas has different sets of pipettes and all procedures were performed using plugged pipette
703 tips. DNA extraction was performed twice on different days. Positive (DNA extracted from
704 blood from patients with known *P. vivax* infection) and negative (no DNA and DNA extracted
705 from individuals who have never traveled to malaria-endemic areas) controls were used in
706 each round of amplification. DNA extracted from blood of a patient with high parasitemia for
707 *P. vivax* and DNA of *P. simium* of a non-human primate with an acute infection and
708 parasitemia confirmed by optical microscopy served as positive controls in the PCR assays.
Primer sequences are provided in Figure S28 and S32.

709
710
711
712
713
714
715
716
717
718
719
720
721
722

Structural modelling of DBP1 and RBP2a genes

RaptorX [91] was used for prediction of secondary structure and protein disorder. Homology models for the DBL domain of *P. vivax* P01 strain, *P. simium* AF22, and the previously published CDC *P. simium* strain were produced by SWISS-MODEL [92], using the crystallographic structure of the DBL domain from *Plasmodium vivax* DBP bound to the ectodomain of the human DARC receptor (PDB ID 4nuv), with an identity of 98%, 96% and 96% for *P. vivax*, *P. simium* AF22 and *P. simium* CDC, respectively. QMEAN values were -2.27, -2.04 and -2.03, respectively. The homology model for the reticulocyte binding protein 2 (RBP2a) of *P. vivax* strain P01 was produced based on the cryoEM structure of the complex between the *P. vivax* RBP2b and the human transferrin receptor TfR1 (PDB ID 6d05)[36], with an identity of 31% and QMEAN value of -2.46. The visualization and structural analysis of the produced models was done with PyMOL (https://pymol.org/2/).

723
724
725
726
727

Data availability

The reference genome assembly and short sequence reads have been uploaded to European Nucleotide Archive (https://www.ebi.ac.uk/ena/) under the Study accession number PRJEB34061.

728
729
730

Acknowledgements

731
732
733
734
735
736
737
738
739
740
741
742

We thank Prof. Xin-zhuan Su at the National Institute of Allergy and Infectious Diseases, NIH, for invaluable help in obtaining the parasite gDNA from the BEI Resources; Sidnei Silva and Graziela Zanini, for assistance on the parasitological diagnosis of the human samples; Aline Lavigne and Larissa Gomes for undertaking the PCR for *P vivax*; Alcides Pissinatti and Silvia Bahadian Moreira for the facilities provided at the Primate Centre of Rio de Janeiro; Orzinete Rodrigues Soares for non-human primates' blood slides'; Marcelo Quintela, Waldemir Paixão Vargas, Carlos Alberto C. da Silva, Alexandre B. de Souza, Vicente Klonowski, Romenique L. Araújo, Luis R. Nogueira, Fernando Barreto, Ana L. Quijada, Luiz P.P. Silva, Gelson Medeiros, Adilson B. Ramos, Marcilene B. Ramos, Carlos A.A. Júnior, Paulo G. Barbosa, Sérgio F. Fragoso, Adilson R. Silva, Cecília Cronemberger, Marcelo Rheingantz, Leonardo Nascimento and João Marins for the field support; *Grupo Técnico de Vigilância de Arboviroses* (GT-Arbo – Brazilian Ministry of Health) for field and

material supports; and Cassio Leonel Peterka from The Brazilian Ministry of Health for malaria epidemiological data. The following reagent was obtained through BEI Resources, NIAID, NIH: *Plasmodium simium*, Strain Howler, MRA-353, contributed by William E. Collins. The work was supported by the King Abdullah University of Science and Technology (KAUST) through the baseline fund BRF1020/01/01 to AP and BAS/1/1056-01-01 to STA, and the Award No. URF/1/1976-25 from the Office of Sponsored Research (OSR). The field work in the Atlantic Forest and laboratory analysis in Brazil received financial support from the Secretary for Health Surveillance of the Ministry of Health through the Global Fund (agreement IOC-005-Fio-13), *Programa Nacional de Excelência (PRONEX)* and contract 407873/2018-0 of the *Conselho Nacional de Desenvolvimento Científico e Tecnológico (CNPq)*, the *Fundação de Amparo à Pesquisa do Estado de Minas Gerais (Fapemig* CBB-APQ-02620-15*)* and the *Fundação Carlos Chagas Filho de Amparo à Pesquisa do Estado do Rio de Janeiro (Faperj)*, Brazil. CNPq supports CFAB, CTDR, MFFC, PB and RLO, with a research productivity fellowship. CTDR (CNE: E-26/202.921/2018), MFFC, PB and RLO are also supported by Faperj as *Cientistas do nosso estado.* AdP-C was supported by a postdoctoral fellowship from the Faperj and DAMA by a fellowship from the CGZV-SVS (Brazilian Ministry of Health) TED 49/2018 grant. SF was supported by a Wellcome Seed Award in Science to DCJ (208965/Z/17/Z).

Author contributions

CTDR, PB, AdPC, RLdO, RC and AP conceived the study. CTDR, PB, CFAdB, MdFFdC, RC and AP supervised and co-ordinated the study. AdPC, FVSdA, DAMA, CBJ, JCdSJ and ZMBH collected materials. OD, QG, AdPC, CFAdB, MdFFdC, FVSdA, DAMA, CBJ, JCsSJ and ZMBH conducted wet-lab experiments. TM, AK, SF, DCJ, FJGV, SA, CTDR, PB, RLdO, CFAdB, MdFFdC, FVSdA, DAMA, CBJ, JCdSJ, ZMBH, RC and AP analysed and interpreted the data. TM, RC, AP, CTDR, PB, CFAdB and RLdO drafted and edited the manuscript. All authors read and approved the final manuscript.

References

776 1 Brasil, P. *et al.* Outbreak of human malaria caused by Plasmodium simium in the Atlantic
777 Forest in Rio de Janeiro: a molecular epidemiological investigation. *Lancet Glob Health* **5**,
778 e1038-e1046, doi:10.1016/S2214-109X(17)30333-9 (2017).

779 2 Cox-Singh, J. *et al.* Plasmodium knowlesi malaria in humans is widely distributed and
780 potentially life threatening. *Clinical infectious diseases : an official publication of the*
781 *Infectious Diseases Society of America* **46**, 165-171, doi:10.1086/524888 (2008).

782 3 Imwong, M. *et al.* Asymptomatic Natural Human Infections With the Simian Malaria
783 Parasites Plasmodium cynomolgi and Plasmodium knowlesi. *J Infect Dis* **219**, 695-702,
784 doi:10.1093/infdis/jiy519 (2019).

785 4 Loy, D. E. *et al.* Out of Africa: origins and evolution of the human malaria parasites
786 Plasmodium falciparum and Plasmodium vivax. *Int J Parasitol* **47**, 87-97,
787 doi:10.1016/j.ijpara.2016.05.008 (2017).

788 5 Liu, W. *et al.* Origin of the human malaria parasite Plasmodium falciparum in gorillas. *Nature*
789 **467**, 420-425, doi:10.1038/nature09442 (2010).

790 6 Liu, W. *et al.* African origin of the malaria parasite Plasmodium vivax. *Nature*
791 *communications* **5**, 3346, doi:10.1038/ncomms4346 (2014).

792 7 Marques, G. R., Condino, M. L., Serpa, L. L. & Cursino, T. V. [Epidemiological aspects of
793 autochthonous malaria in the Atlantic forest area of the northern coast of the State of Sao
794 Paulo, 1985-2006]. *Rev Soc Bras Med Trop* **41**, 386-389 (2008).

795 8 Cox-Singh, J. *et al.* Plasmodium knowlesi malaria in humans is widely distributed and
796 potentially life threatening. *Clin Infect Dis* **46**, 165-171, doi:10.1086/524888 (2008).

797 9 Ta, T. H. *et al.* First case of a naturally acquired human infection with Plasmodium
798 cynomolgi. *Malar J* **13**, 68, doi:10.1186/1475-2875-13-68 (2014).

799 10 Marchand, R. P., Culleton, R., Maeno, Y., Quang, N. T. & Nakazawa, S. Co-infections of
800 Plasmodium knowlesi, P. falciparum, and P. vivax among Humans and Anopheles dirus
801 Mosquitoes, Southern Vietnam. *Emerg Infect Dis* **17**, 1232-1239, doi:10.3201/eid1707.101551
802 (2011).

803 11 Otto, T. D. *et al.* Genomes of all known members of a Plasmodium subgenus reveal paths to
804 virulent human malaria. *Nature microbiology* **3**, 687-697, doi:10.1038/s41564-018-0162-2
805 (2018).

806 12 de Pina-Costa, A. *et al.* Malaria in Brazil: what happens outside the Amazonian endemic
807 region. *Mem Inst Oswaldo Cruz* **109**, 618-633, doi:10.1590/0074-0276140228 (2014).

808 13 Collins, W. E., Contacos, P. G. & Guinn, E. G. Observations on the sporogonic cycle and
809 transmission of Plasmodium simium Da Fonseca. *J Parasitol* **55**, 814-816 (1969).

810 14 de Alvarenga, D. A. M. *et al.* An assay for the identification of Plasmodium simium infection
811 for diagnosis of zoonotic malaria in the Brazilian Atlantic Forest. *Scientific reports* **8**, 86,
812 doi:10.1038/s41598-017-18216-x (2018).

813 15 Escalante, A. A. *et al.* A monkey's tale: the origin of Plasmodium vivax as a human malaria
814 parasite. *Proc Natl Acad Sci U S A* **102**, 1980-1985, doi:10.1073/pnas.0409652102 (2005).

815 16 Gelabert, P. *et al.* Mitochondrial DNA from the eradicated European Plasmodium vivax and P.
816 falciparum from 70-year-old slides from the Ebro Delta in Spain. *Proceedings of the National*
817 *Academy of Sciences of the United States of America* **113**, 11495-11500,
818 doi:10.1073/pnas.1611017113 (2016).

819 17 Rodrigues, P. T. *et al.* Human migration and the spread of malaria parasites to the New World.
820 *Scientific reports* **8**, 1993, doi:10.1038/s41598-018-19554-0 (2018).

821 18 Deane, L. M. Simian malaria in Brazil. *Mem Inst Oswaldo Cruz* **87 Suppl 3**, 1-20 (1992).

822 19 Fonseca, F. [Plasmodium of a primate of Brazil]. *Mem Inst Oswaldo Cruz* **49**, 543-553 (1951).

823 20 Leclerc, M. C. *et al.* Meager genetic variability of the human malaria agent Plasmodium
824 vivax. *Proceedings of the National Academy of Sciences of the United States of America* **101**,
825 14455-14460, doi:10.1073/pnas.0405186101 (2004).

826 21 Duarte, A. M. *et al.* Widespread occurrence of antibodies against circumsporozoite protein
827 and against blood forms of Plasmodium vivax, P. falciparum and P. malariae in Brazilian wild
828 monkeys. *J Med Primatol* **35**, 87-96, doi:10.1111/j.1600-0684.2006.00148.x (2006).

829 22 Tazi, L. & Ayala, F. J. Unresolved direction of host transfer of Plasmodium vivax v. P.
830 simium and P. malariae v. P. brasilianum. *Infect Genet Evol* **11**, 209-221,
831 doi:10.1016/j.meegid.2010.08.007 (2011).

832 23 Coatney, G. R., Collins, W. E., Warren, M. & Contacos, P. G. in *The Primate Malarias*
833 (National Institutes of Health, 1971).

834 24 Auburn, S. *et al.* A new Plasmodium vivax reference sequence with improved assembly of the
835 subtelomeres reveals an abundance of pir genes. *Wellcome Open Res* **1**, 4,
836 doi:10.12688/wellcomeopenres.9876.1 (2016).

837 25 Hupalo, D. N. *et al.* Population genomics studies identify signatures of global dispersal and
838 drug resistance in Plasmodium vivax. *Nat Genet* **48**, 953-958, doi:10.1038/ng.3588 (2016).

839 26 Alexander, D. H., Novembre, J. & Lange, K. Fast model-based estimation of ancestry in
840 unrelated individuals. *Genome research* **19**, 1655-1664, doi:10.1101/gr.094052.109 (2009).

841 27 Willing, E. M., Dreyer, C. & van Oosterhout, C. Estimates of genetic differentiation measured
842 by F(ST) do not necessarily require large sample sizes when using many SNP markers. *PloS*
843 *one* **7**, e42649, doi:10.1371/journal.pone.0042649 (2012).

844 28 Cunningham, D., Lawton, J., Jarra, W., Preiser, P. & Langhorne, J. The pir multigene family
845 of Plasmodium: antigenic variation and beyond. *Mol Biochem Parasitol* **170**, 65-73,
846 doi:10.1016/j.molbiopara.2009.12.010 (2010).

847 29 Warncke, J. D., Vakonakis, I. & Beck, H. P. Plasmodium Helical Interspersed Subtelomeric
848 (PHIST) Proteins, at the Center of Host Cell Remodeling. *Microbiol Mol Biol Rev* **80**, 905-
849 927, doi:10.1128/MMBR.00014-16 (2016).

850 30 Castillo, A. I., Andreina Pacheco, M. & Escalante, A. A. Evolution of the merozoite surface
851 protein 7 (msp7) family in Plasmodium vivax and P. falciparum: A comparative approach.
852 *Infect Genet Evol* **50**, 7-19, doi:10.1016/j.meegid.2017.01.024 (2017).

853 31 Ntumngia, F. B. *et al.* Characterisation of a tryptophan-rich Plasmodium falciparum antigen
854 associated with merozoites. *Mol Biochem Parasitol* **137**, 349-353,
855 doi:10.1016/j.molbiopara.2004.06.008 (2004).

856 32 Kanjee, U., Rangel, G. W., Clark, M. A. & Duraisingh, M. T. Molecular and cellular
857 interactions defining the tropism of Plasmodium vivax for reticulocytes. *Curr Opin Microbiol*
858 **46**, 109-115, doi:10.1016/j.mib.2018.10.002 (2018).

859 33 Miller, L. H., McAuliffe, F. M. & Mason, S. J. Erythrocyte receptors for malaria merozoites.
860 *Am J Trop Med Hyg* **26**, 204-208, doi:10.4269/ajtmh.1977.26.204 (1977).

861 34 Iyer, J., Gruner, A. C., Renia, L., Snounou, G. & Preiser, P. R. Invasion of host cells by
862 malaria parasites: a tale of two protein families. *Mol Microbiol* **65**, 231-249,
863 doi:10.1111/j.1365-2958.2007.05791.x (2007).

864 35 Chan, L. J., Dietrich, M. H., Nguitragool, W. & Tham, W. H. Plasmodium vivax Reticulocyte
865 Binding Proteins for invasion into reticulocytes. *Cell Microbiol*, e13110,
866 doi:10.1111/cmi.13110 (2019).

867 36 Gruszczyk, J. *et al.* Cryo-EM structure of an essential Plasmodium vivax invasion complex.
868 *Nature* **559**, 135-139, doi:10.1038/s41586-018-0249-1 (2018).

869 37 Carlton, J. M. *et al.* Comparative genomics of the neglected human malaria parasite
870 Plasmodium vivax. *Nature* **455**, 757-763, doi:10.1038/nature07327 (2008).

871 38 Gilabert, A. *et al.* Plasmodium vivax-like genome sequences shed new insights into
872 Plasmodium vivax biology and evolution. *PLoS Biol* **16**, e2006035,
873 doi:10.1371/journal.pbio.2006035 (2018).

874 39 Ntumngia, F. B. *et al.* Genetic variation among Plasmodium vivax isolates adapted to non-
875 human primates and the implication for vaccine development. *Am J Trop Med Hyg* **80**, 218-
876 227 (2009).

877 40 Rausch, T. *et al.* DELLY: structural variant discovery by integrated paired-end and split-read
878 analysis. *Bioinformatics* **28**, i333-i339, doi:10.1093/bioinformatics/bts378 (2012).

879 41 Batchelor, J. D., Zahm, J. A. & Tolia, N. H. Dimerization of Plasmodium vivax DBP is
880 induced upon receptor binding and drives recognition of DARC. *Nat Struct Mol Biol* **18**, 908-
881 914, doi:10.1038/nsmb.2088 (2011).

882 42 Jeffares, D. C., Tomiczek, B., Sojo, V. & dos Reis, M. A beginners guide to estimating the
883 non-synonymous to synonymous rate ratio of all protein-coding genes in a genome. *Methods*
884 *Mol Biol* **1201**, 65-90, doi:10.1007/978-1-4939-1438-8_4 (2015).

885 43 Proto, W. R. *et al.* Adaptation of Plasmodium falciparum to humans involved the loss of an
886 ape-specific erythrocyte invasion ligand. *Nature communications* **10**, 4512,
887 doi:10.1038/s41467-019-12294-3 (2019).

888 44 Wright, P. E. & Dyson, H. J. Intrinsically disordered proteins in cellular signalling and
889 regulation. *Nature reviews. Molecular cell biology* **16**, 18-29, doi:10.1038/nrm3920 (2015).

890 45 Culleton, R. & Carter, R. African Plasmodium vivax: distribution and origins. *Int J Parasitol*
891 **42**, 1091-1097, doi:10.1016/j.ijpara.2012.08.005 (2012).

892 46 Li, J. *et al.* Geographic subdivision of the range of the malaria parasite Plasmodium vivax.
893 *Emerging infectious diseases* **7**, 35-42, doi:10.3201/eid0701.010105 (2001).

894 47 Choi, E. H., Lee, S. K., Ihm, C. & Sohn, Y. H. Rapid DNA extraction from dried blood spots
895 on filter paper: potential applications in biobanking. *Osong Public Health Res Perspect* **5**,
896 351-357, doi:10.1016/j.phrp.2014.09.005 (2014).

897 48 Bolger, A. M., Lohse, M. & Usadel, B. Trimmomatic: a flexible trimmer for Illumina
898 sequence data. *Bioinformatics* **30**, 2114-2120, doi:10.1093/bioinformatics/btu170 (2014).

899 49 Langmead, B. & Salzberg, S. L. Fast gapped-read alignment with Bowtie 2. *Nature methods*
900 **9**, 357-359, doi:10.1038/nmeth.1923 (2012).

901 50 Bankevich, A. *et al.* SPAdes: a new genome assembly algorithm and its applications to single-
902 cell sequencing. *J Comput Biol* **19**, 455-477, doi:10.1089/cmb.2012.0021 (2012).

903 51 Boetzer, M., Henkel, C. V., Jansen, H. J., Butler, D. & Pirovano, W. Scaffolding pre-
904 assembled contigs using SSPACE. *Bioinformatics* **27**, 578-579,
905 doi:10.1093/bioinformatics/btq683 (2011).

906 52 Boetzer, M. & Pirovano, W. Toward almost closed genomes with GapFiller. *Genome biology*
907 **13**, R56, doi:10.1186/gb-2012-13-6-r56 (2012).

908 53 Walker, B. J. *et al.* Pilon: an integrated tool for comprehensive microbial variant detection and
909 genome assembly improvement. *PloS one* **9**, e112963, doi:10.1371/journal.pone.0112963
910 (2014).

911 54 Laetsch, D. & Blaxter, M. BlobTools: Interrogation of genome assemblies [version 1;
912 referees: 2 approved with reservations]. *F1000Research* **6**,
913 doi:10.12688/f1000research.12232.1 (2017).

914 55 Jongwutiwes, S. *et al.* Mitochondrial genome sequences support ancient population expansion
915 in Plasmodium vivax. *Molecular biology and evolution* **22**, 1733-1739,
916 doi:10.1093/molbev/msi168 (2005).

917 56 Rodrigues, P. T. *et al.* Using mitochondrial genome sequences to track the origin of imported
918 Plasmodium vivax infections diagnosed in the United States. *Am J Trop Med Hyg* **90**, 1102-
919 1108, doi:10.4269/ajtmh.13-0588 (2014).

920 57 Bandelt, H. J., Forster, P. & Rohl, A. Median-joining networks for inferring intraspecific
921 phylogenies. *Molecular biology and evolution* **16**, 37-48,
922 doi:10.1093/oxfordjournals.molbev.a026036 (1999).

923 58 Leigh, J. W. & Bryant, D. POPART: full-feature software for haplotype network construction.
924 *Methods Ecol Evol* **6**, 1110-1116, doi:10.1111/2041-210x.12410 (2015).

925 59 Holt, C. & Yandell, M. MAKER2: an annotation pipeline and genome-database management
926 tool for second-generation genome projects. *BMC Bioinformatics* **12**, 491, doi:10.1186/1471-
927 2105-12-491 (2011).

928 60 Steinbiss, S. *et al.* Companion: a web server for annotation and analysis of parasite genomes.
929 *Nucleic acids research* **44**, W29-34, doi:10.1093/nar/gkw292 (2016).

930 61 Waterhouse, R. M. *et al.* BUSCO applications from quality assessments to gene prediction
931 and phylogenomics. *Molecular biology and evolution*, doi:10.1093/molbev/msx319 (2017).

932 62 Simao, F. A., Waterhouse, R. M., Ioannidis, P., Kriventseva, E. V. & Zdobnov, E. M.
933 BUSCO: assessing genome assembly and annotation completeness with single-copy
934 orthologs. *Bioinformatics* **31**, 3210-3212, doi:10.1093/bioinformatics/btv351 (2015).

935 63 Lechner, M. *et al.* Proteinortho: detection of (co-)orthologs in large-scale analysis. *BMC*
936 *Bioinformatics* **12**, 124, doi:10.1186/1471-2105-12-124 (2011).

937 64 Katoh, K. & Standley, D. M. MAFFT multiple sequence alignment software version 7:
938 improvements in performance and usability. *Molecular biology and evolution* **30**, 772-780,
939 doi:10.1093/molbev/mst010 (2013).

940 65 Capella-Gutierrez, S., Silla-Martinez, J. M. & Gabaldon, T. trimAl: a tool for automated
941 alignment trimming in large-scale phylogenetic analyses. *Bioinformatics* **25**, 1972-1973,
942 doi:10.1093/bioinformatics/btp348 (2009).

943 66 Stamatakis, A. RAxML version 8: a tool for phylogenetic analysis and post-analysis of large
944 phylogenies. *Bioinformatics* **30**, 1312-1313, doi:10.1093/bioinformatics/btu033 (2014).

945 67 Sedlazeck, F. J., Rescheneder, P. & von Haeseler, A. NextGenMap: fast and accurate read
946 mapping in highly polymorphic genomes. *Bioinformatics* **29**, 2790-2791,
947 doi:10.1093/bioinformatics/btt468 (2013).

948 68 Li, H. *et al.* The Sequence Alignment/Map format and SAMtools. *Bioinformatics* **25**, 2078-
949 2079, doi:btp352 [pii]
950 10.1093/bioinformatics/btp352 (2009).

951 69 McKenna, A. *et al.* The Genome Analysis Toolkit: a MapReduce framework for analyzing
952 next-generation DNA sequencing data. *Genome research* **20**, 1297-1303,
953 doi:10.1101/gr.107524.110 (2010).

954 70 Garrison, E. & Marth, G. Haplotype-based variant detection from short-read sequencing.
955 *arXiv*, 1207.3907 (2012).

956 71 Chang, C. C. *et al.* Second-generation PLINK: rising to the challenge of larger and richer
957 datasets. *Gigascience* **4**, 7, doi:10.1186/s13742-015-0047-8 (2015).

958 72 Pfeifer, B., Wittelsburger, U., Ramos-Onsins, S. E. & Lercher, M. J. PopGenome: an efficient
959 Swiss army knife for population genomic analyses in R. *Molecular biology and evolution* **31**,
960 1929-1936, doi:10.1093/molbev/msu136 (2014).

961 73 R Development Core Team. R: A language and environment for statistical computing. R
962 Foundation for Statistical Computing, Vienna, Austria. ISBN 3-900051-07-0, URL
963 http://www.R-project.org. (2007).

964 74 Weir, B. S. & Cockerham, C. C. Estimating F-Statistics for the Analysis of Population
965 Structure. *Evolution* **38**, 1358-1370, doi:10.1111/j.1558-5646.1984.tb05657.x (1984).

966 75 Cingolani, P. *et al.* A program for annotating and predicting the effects of single nucleotide
967 polymorphisms, SnpEff: SNPs in the genome of Drosophila melanogaster strain w1118; iso-2;
968 iso-3. *Fly (Austin)* **6**, 80-92, doi:10.4161/fly.19695 (2012).

969 76 Guindon, S. *et al.* New algorithms and methods to estimate maximum-likelihood phylogenies:
970 assessing the performance of PhyML 3.0. *Syst Biol* **59**, 307-321, doi:10.1093/sysbio/syq010
971 (2010).

972 77 Guindon, S. & Gascuel, O. A simple, fast, and accurate algorithm to estimate large
973 phylogenies by maximum likelihood. *Syst Biol* **52**, 696-704, doi:10.1080/10635150390235520
974 (2003).

975 78 Lefort, V., Longueville, J. E. & Gascuel, O. SMS: Smart Model Selection in PhyML.
976 *Molecular biology and evolution* **34**, 2422-2424, doi:10.1093/molbev/msx149 (2017).

977 79 Anisimova, M., Gil, M., Dufayard, J. F., Dessimoz, C. & Gascuel, O. Survey of branch
978 support methods demonstrates accuracy, power, and robustness of fast likelihood-based
979 approximation schemes. *Syst Biol* **60**, 685-699, doi:10.1093/sysbio/syr041 (2011).

980 80 Huson, D. H. & Bryant, D. Application of phylogenetic networks in evolutionary studies.
981 *Molecular biology and evolution* **23**, 254-267, doi:10.1093/molbev/msj030 (2006).

982 81 Bryant, D. & Moulton, V. Neighbor-net: an agglomerative method for the construction of
983 phylogenetic networks. *Molecular biology and evolution* **21**, 255-265,
984 doi:10.1093/molbev/msh018 (2004).

985 82 Larkin, M. A. *et al.* Clustal W and Clustal X version 2.0. *Bioinformatics* **23**, 2947-2948,
986 doi:10.1093/bioinformatics/btm404 (2007).

987 83 Thompson, J. D., Higgins, D. G. & Gibson, T. J. CLUSTAL W: improving the sensitivity of
988 progressive multiple sequence alignment through sequence weighting, position-specific gap
989 penalties and weight matrix choice. *Nucleic acids research* **22**, 4673-4680 (1994).

990 84 Chaisson, M. J. & Tesler, G. Mapping single molecule sequencing reads using basic local
991 alignment with successive refinement (BLASR): application and theory. *BMC Bioinformatics*
992 **13**, 238, doi:10.1186/1471-2105-13-238 (2012).

993 85 Seibt, K. M., Schmidt, T. & Heitkam, T. FlexiDot: highly customizable, ambiguity-aware
994 dotplots for visual sequence analyses. *Bioinformatics* **34**, 3575-3577,
995 doi:10.1093/bioinformatics/bty395 (2018).

996 86 van Ooij, C. *et al.* The malaria secretome: from algorithms to essential function in blood stage
997 infection. *PLoS pathogens* **4**, e1000084, doi:10.1371/journal.ppat.1000084 (2008).

998 87 Boddey, J. A. *et al.* Role of plasmepsin V in export of diverse protein families from the
999 Plasmodium falciparum exportome. *Traffic* **14**, 532-550, doi:10.1111/tra.12053 (2013).

1000 88 Schulze, J. *et al.* The Plasmodium falciparum exportome contains non-canonical PEXEL/HT
1001 proteins. *Mol Microbiol* **97**, 301-314, doi:10.1111/mmi.13024 (2015).

1002 89 Hu, G. *et al.* Transcriptional profiling of growth perturbations of the human malaria parasite
1003 Plasmodium falciparum. *Nat Biotechnol* **28**, 91-98, doi:10.1038/nbt.1597 (2010).

1004 90 Ye, J. *et al.* Primer-BLAST: a tool to design target-specific primers for polymerase chain
1005 reaction. *BMC Bioinformatics* **13**, 134, doi:10.1186/1471-2105-13-134 (2012).

1006 91 Wang, S., Li, W., Liu, S. & Xu, J. RaptorX-Property: a web server for protein structure
1007 property prediction. *Nucleic acids research* **44**, W430-435, doi:10.1093/nar/gkw306 (2016).

92 Waterhouse, A. *et al.* SWISS-MODEL: homology modelling of protein structures and complexes. *Nucleic acids research* **46**, W296-W303, doi:10.1093/nar/gky427 (2018).

Figure Legends

Figure 1 - SNP phylogeny

A) Mid-point rooted maximum likelihood tree produced from 143,123 concatenated SNP positions with data from at least 55 samples. The tree was produced using PhyML with the GTR evolutionary model. Branch support was evaluated with the Bayesian-like transformation of approximate likelihood ratio test (aBayes). Genetic distance shown below tree. *P. vivax* isolates are denoted as colored circles by their country of sample origin. A tree with specific sample IDs is available in Figure S7. B) Magnification of the *P. simium* clade (as in panel A). C) Map denoting the geographic location of *P. simium* samples.

Figure 2 - Nucleotide diversity

Box plot showing the pair-wise nucleotide diversity between human-infecting *P. simium* samples (left), *P. vivax* samples (middle), and between *P. simium* and *P. vivax* samples (right). Diversity is shown for entire genome (left-most plots, blue) and exonic regions only (right-most plots, orange). Individual values from pairwise comparsions are shown as grey dots, boxes denote 25th and 75th percentiles, and whiskers an additional 1.5 interquartile lengths. The observed nucleotide diversity between *P. simium* and *P. vivax* samples is significantly higher than between *P. vivax* samples (Mann-Whitney U, genome; $p=8.79\times10^{-20}$, exons; $p=3.72\times10^{-20}$).

Figure 3 - F_{ST} ratios

A) Gene F_{ST} values were calculated between simium and American vivax samples (x-axis) and American and Asian vivax samples (y-axis). Each dot corresponds to a gene, and the distributions of the two FST measures are shown as bar charts above and to the right of the scatter plot. B) The ratio between F_{ST} values between i) simium and American vivax samples, and ii) American and Asian vivax samples were calculated for each gene (top). A pseudo count of one was added to all F_{ST} values. The distributions of log2-ratios are shown as violin plots (bottom) for all genes (grey),

1042 PIR genes (red), PHIST genes (brown), TRAg genes (turquoise), invasion genes
1043 (yellow), and exported genes (dark blue). Only genes with SNP differences between
1044 the three populations are included in this analysis. F_{ST} values and ratios are provided
1045 in Table S7. P-values from Mann-Whitney U tests for differences in medians between
1046 PIR, PHIST, TRAg, invasion genes, exported genes, and all remaining genes are
1047 indicated on plot (e.g. PIR genes are compared to all non-PIR genes).
1048
1049 **Figure 4 - Invasome deletions**
1050 A) Overview of the invasome gene groups, Reticulocyte Binding Proteins (RBPs) and
1051 Duffy Binding Proteins (DBPs) in *Plasmodium vivax* and *P. simium*. The *P. vivax*
1052 genome harbours two RBP2d genes, one of which is a pseudogene (Table S9). B)
1053 Schematic depiction of samples with and without the deletion found in DBP1.
1054 C) Left: Structural rendering of DBP1, showing known structural domains and motifs.
1055 The two fragment molecules from the human DARC receptor are shown in grey. The
1056 3-dimensional structure of the DBL-DARC complex was modeled based on the *P.*
1057 *vivax* crystallographic model (PDB 4nuv). The region deleted in sequences from
1058 human-infecting *P. simium*, as compared to *P. vivax* P01, is highlighted in red. Right:
1059 Details of DBP1 protein alignments. A full alignment is available in Figure S20.
1060 D) Similar to panel C) but for RBP2a. The complex between the reticulocyte binding
1061 domain and the human receptor was modeled based on the cryoEM structure of the
1062 complex between the *P. vivax* RBP2b and the human transferrin receptor TfR1 (PDB
1063 6d05). A full alignment is available in Figure S21.
1064
1065

Figure 1

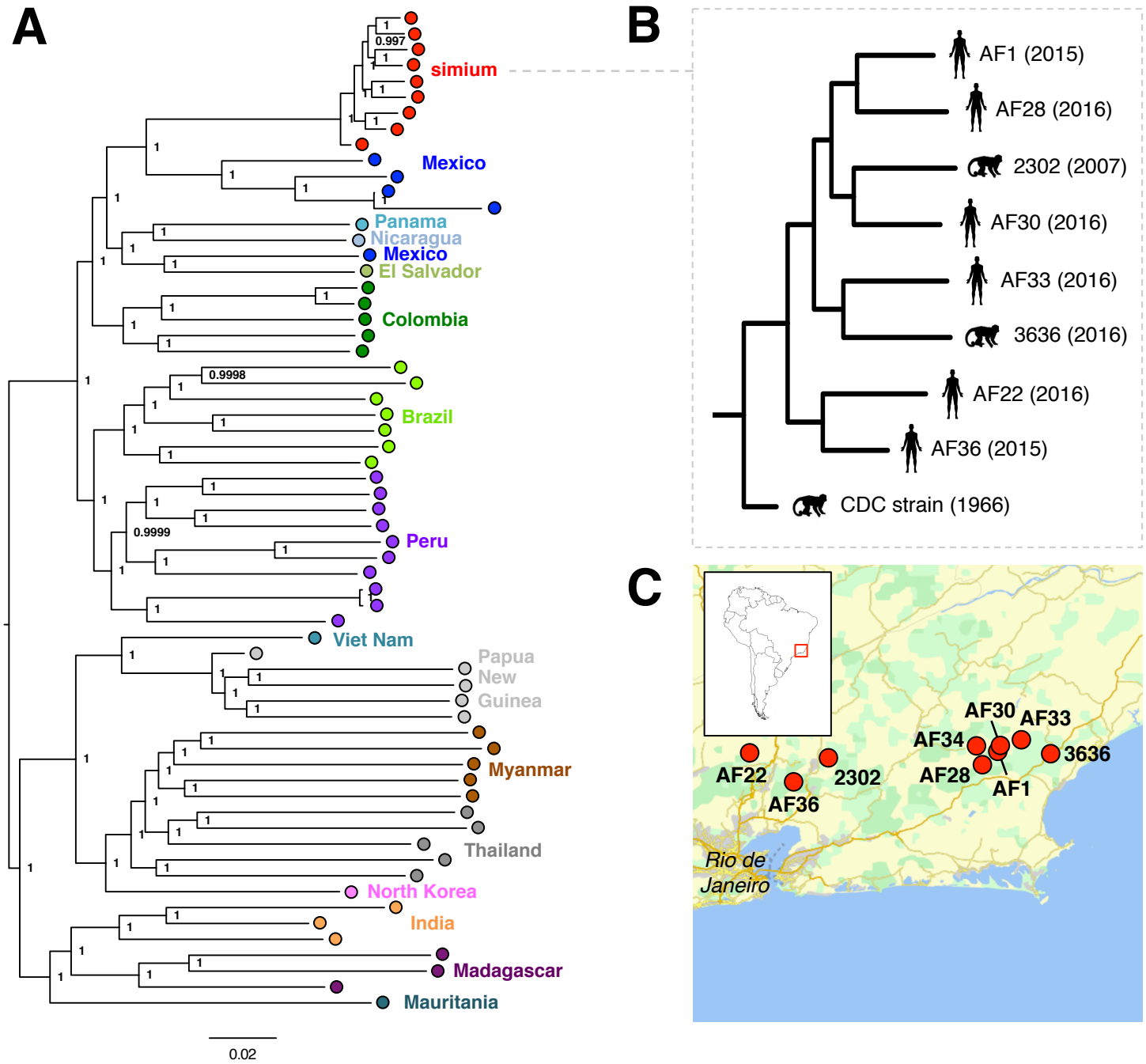
A
simium
Mexico
Panama
Nicaragua
Mexico
El Salvador
Colombia
Brazil
Peru
Viet Nam
Papua
New
Guinea
Myanmar
Thailand
North Korea
India
Madagascar
Mauritania
0.997
0.9998
0.9999
0.02
B
AF1 (2015)
AF28 (2016)
2302 (2007)
AF30 (2016)
AF33 (2016)
3636 (2016)
AF22 (2016)
AF36 (2015)
CDC strain (1966)
C
AF22
AF36
2302
AF30
AF33
AF34
AF28
AF1
3636
Rio de
Janeiro

Figure 2

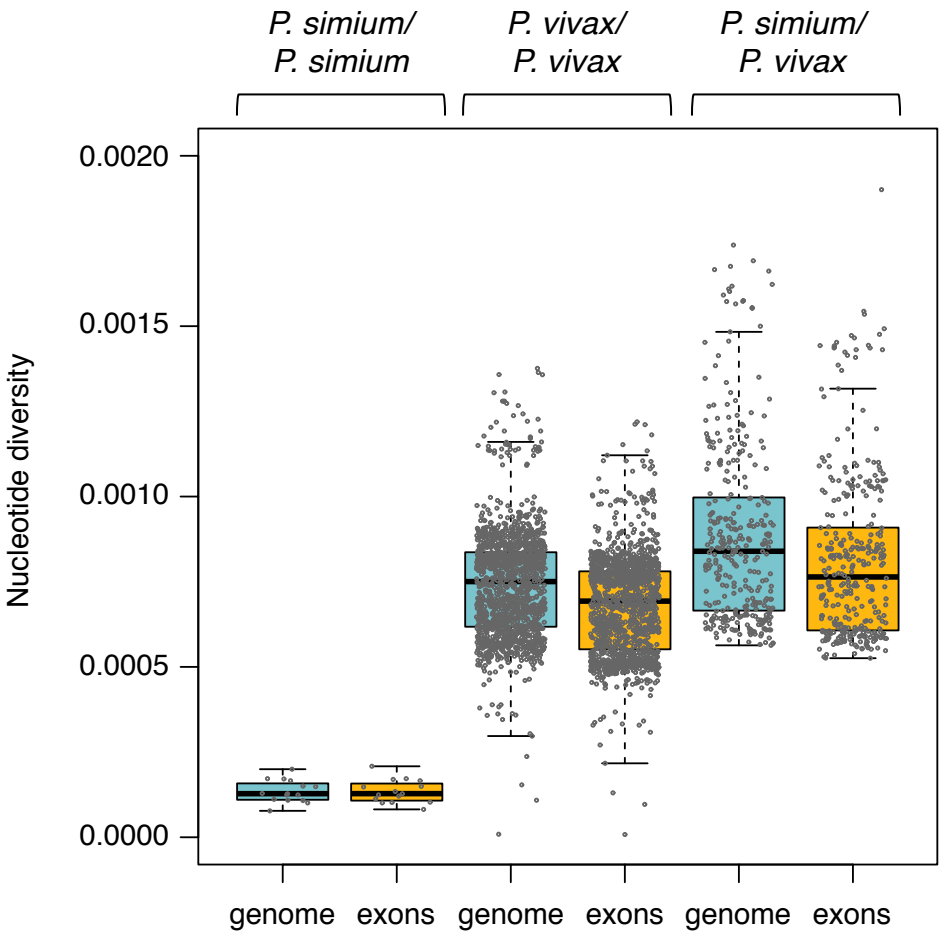
P. simium/
P. simium
P. vivax/
P. vivax
P. simium/
P. vivax
Nucleotide diversity
0.0020
0.0015
0.0010
0.0005
0.0000
genome
exons
genome
exons
genome
exons

Figure 3

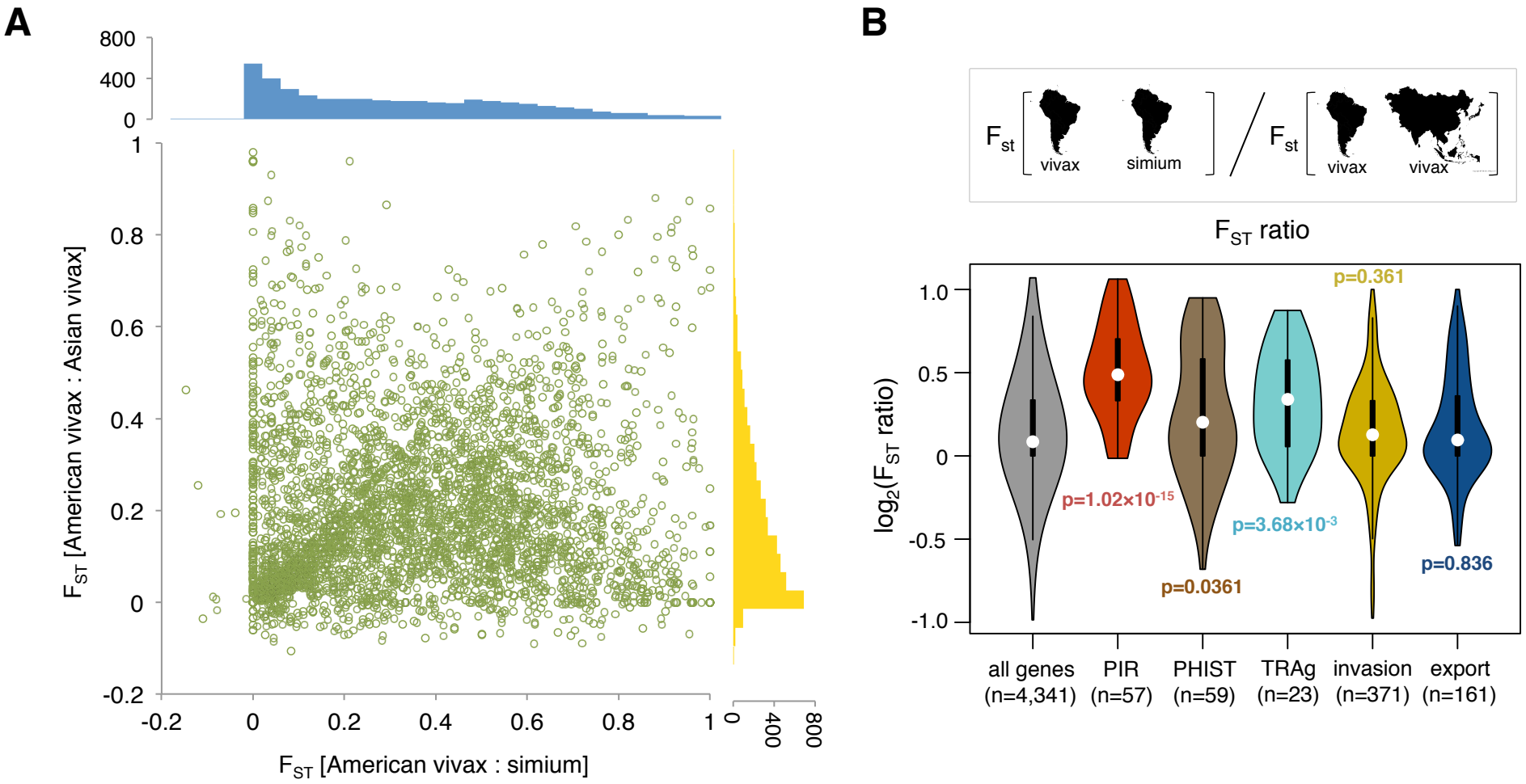
A
800
400
0
1
0.8
0.6
0.4
0.2
0
-0.2
-0.2
0
0.2
0.4
0.6
0.8
1
0
400
800
F_ST [American vivax : Asian vivax]
F_ST [American vivax : simium]
B
F_st
vivax
simium
F_st
vivax
vivax
F_ST ratio
log2(F_ST ratio)
1.0
0.5
0
-0.5
-1.0
p=0.361
p=1.02×10^-15
p=3.68×10^-3
p=0.0361
p=0.836
all genes (n=4,341)
PIR (n=57)
PHIST (n=59)
TRAg (n=23)
invasion (n=371)
export (n=161)

Figure 4

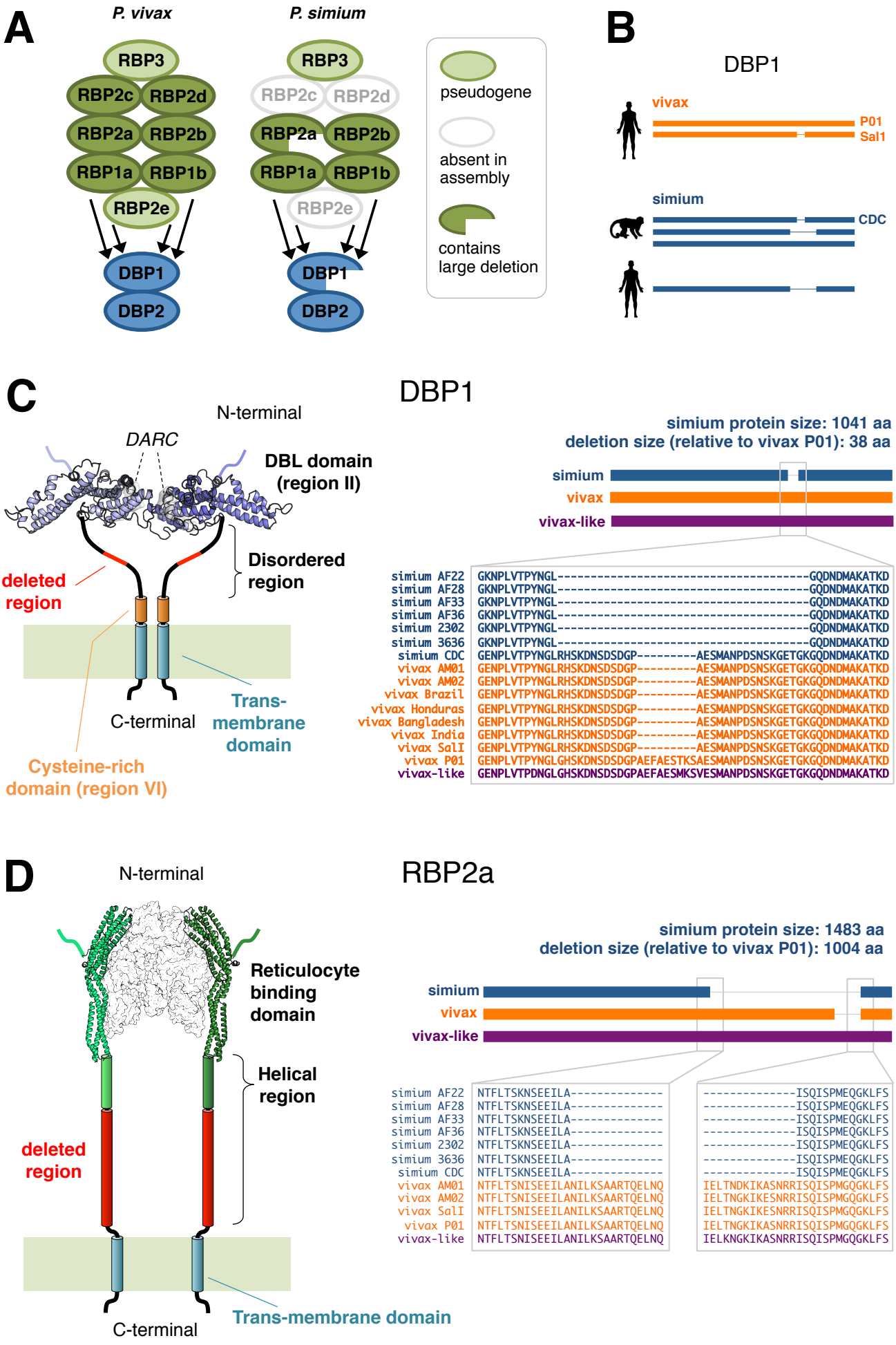
A
P. vivax
P. simium
RBP3
RBP2c
RBP2d
RBP2a
RBP2b
RBP1a
RBP1b
RBP2e
DBP1
DBP2
pseudogene
absent in assembly
contains large deletion
B
DBP1
vivax
P01
Sal1
simium
CDC
C
DBP1
N-terminal
DARC
DBL domain (region II)
Disordered region
deleted region
Trans-membrane domain
C-terminal
Cysteine-rich domain (region VI)
simium protein size: 1041 aa
deletion size (relative to vivax P01): 38 aa
simium
vivax
vivax-like
simium AF22 GKNPLVTPYNGL----------GQDNDMAKATKD
simium AF28 GKNPLVTPYNGL----------GQDNDMAKATKD
simium AF33 GKNPLVTPYNGL----------GQDNDMAKATKD
simium AF36 GKNPLVTPYNGL----------GQDNDMAKATKD
simium 2302 GKNPLVTPYNGL----------GQDNDMAKATKD
simium 3636 GKNPLVTPYNGL----------GQDNDMAKATKD
simium CDC GENPLVTPYNGLRHSKDNSDSDGP---------AESMANPDSNSKGETGKGQDNDMAKATKD
vivax AM01 GENPLVTPYNGLRHSKDNSDSDGP---------AESMANPDSNSKGETGKGQDNDMAKATKD
vivax AM02 GENPLVTPYNGLRHSKDNSDSDGP---------AESMANPDSNSKGETGKGQDNDMAKATKD
vivax Brazil GENPLVTPYNGLRHSKDNSDSDGP---------AESMANPDSNSKGETGKGQDNDMAKATKD
vivax Honduras GENPLVTPYNGLRHSKDNSDSDGP---------AESMANPDSNSKGETGKGQDNDMAKATKD
vivax Bangladesh GENPLVTPYNGLRHSKDNSDSDGP---------AESMANPDSNSKGETGKGQDNDMAKATKD
vivax India GENPLVTPYNGLRHSKDNSDSDGP---------AESMANPDSNSKGETGKGQDNDMAKATKD
vivax SalI GENPLVTPYNGLRHSKDNSDSDGP---------AESMANPDSNSKGETGKGQDNDMAKATKD
vivax P01 GENPLVTPYNGLGHSKDNSDSDGPAEFAESTKSAESMANPDSNSKGETGKGQDNDMAKATKD
vivax-like GENPLVTPDNGLGHSKDNSDSDGPAEFAESMKSVESMANPDSNSKGETGKGQDNDMAKATKD
D
N-terminal
RBP2a
Reticulocyte binding domain
Helical region
deleted region
C-terminal
Trans-membrane domain
simium protein size: 1483 aa
deletion size (relative to vivax P01): 1004 aa
simium
vivax
vivax-like
simium AF22 NTFLTSKNSEEILA---------- ----------ISQISPMEQGKLFS
simium AF28 NTFLTSKNSEEILA---------- ----------ISQISPMEQGKLFS
simium AF33 NTFLTSKNSEEILA---------- ----------ISQISPMEQGKLFS
simium AF36 NTFLTSKNSEEILA---------- ----------ISQISPMEQGKLFS
simium 2302 NTFLTSKNSEEILA---------- ----------ISQISPMEQGKLFS
simium 3636 NTFLTSKNSEEILA---------- ----------ISQISPMEQGKLFS
simium CDC NTFLTSKNSEEILA---------- ----------ISQISPMEQGKLFS
vivax AM01 NTFLTSNISEEILANILKSAARTQELNQ IELTNDKIKASNRRISQISPMGQGKLFS
vivax AM02 NTFLTSNISEEILANILKSAARTQELNQ IELTNGKIKESNRRISQISPMGQGKLFS
vivax SalI NTFLTSNISEEILANILKSAARTQELNQ IELTNGKIKESNRRISQISPMGQGKLFS
vivax P01 NTFLTSNISEEILANILKSAARTQELNQ IELTNGKIKASNRRISQISPMGQGKLFS
vivax-like NTFLTSNISEEILANILKSAARTQELNQ IELKNGKIKASNRRISQISPMGQGKLFS